The role of ligand to metal charge-transfer states on the luminescence of Europium complexes with 18-membered macrocyclic ligands[i]

Aline Nonat[a], David Esteban-Gómez[b], Laura Valencia[c], Paulo Pérez-Lourido[c], José Luis Barriada[b], Loïc J. Charbonnière[a*] and Carlos Platas-Iglesias[b†]

[a] Synthèse pour l'Analyse (SynPA), Institut Pluridisciplinaire Hubert Curien (IPHC, UMR 7178, CNRS/Université de Strasbourg), ECPM, 25 rue Becquerel, 67087 Strasbourg Cedex, France

[b] Centro de Investigacións Científicas Avanzadas (CICA) and Departamento de Química, Universidade da Coruña, Campus da Zapateira-Rúa da Fraga 10, 15008 A Coruña, Spain

[c] Departamento de Química Inorgánica, Facultad de Ciencias, Universidade de Vigo, As Lagoas, Marcosende, 36310 Pontevedra, Spain

Dalton Transactions, volume 48, issue 12, pages 4035–4045, 28 March 2019
Submitted 19 December 2018, accepted 27 February 2019, first published 27 February 2019

How to cite:

A. Nonat, D. Esteban-Gómez, L. Valencia, P. Pérez-Lourido, J. L. Barriada, L. J. Charbonnière and C. Platas-Iglesias, The role of ligand to metal charge-transfer states on the luminescence of Europium complexes with 18-membered macrocyclic ligands, *Dalt. Trans.*, 2019, **48**, 4035–4045. DOI: 10.1039/C8DT05005H.

Abstract

We report a detailed study of the photophysical properties of Eu^{III} and Tb^{III} complexes with two ligands based on a 3,6,10,13-tetraaza-1,8(2,6)-dipyridinacyclotetradecaphane platform containing either four pyridine-2yl-methyl (L^1) or four hydroxyethyl (L^2) pendant arms. The $[TbL^1]^{3+}$ and $[TbL^2]^{3+}$ complexes present moderate luminescence quantum yields upon excitation through the ligand bands ($\phi_{H2}O$ = 7.4 and 21%, respectively). The $[EuL^2]^{3+}$ complex displays a relatively low quantum yield in H_2O ($\phi_{H2}O$ = 1.6%) that increases considerably in D_2O ($\phi_{D2}O$ = 5.3%), which highlights the strong quenching effect of the four ligand O–H oscillators. The emission spectrum of $[EuL^1]^{3+}$ is rather unusual in that it shows a relatively high intensity of the $^5D_0 \rightarrow {}^7F_{5,6}$ transitions, which appears to be also related to the distorted D_{4d} symmetry of the coordination polyhedron. Surprisingly, the quantum yield of the $[EuL^1]^{3+}$ complex is very low ($\phi_{H2}O$ = 0.10%), considering the good protection of the Eu^{III} coordination environment offered by the ligand. Cyclic voltammograms recorded from aqueous solutions of $[EuL^1]^{3+}$ display a reversible curve with a half-wave potential of −620 mV (*versus* Ag/AgCl), while $[EuL^2]^{3+}$ presents a reduction peak at more negative potential (−1040 mV). Thus, the L^1 ligand provides a rather good stabilisation of divalent Eu compared to the L^2 analogue, suggesting that the presence of a low-lying ligand-to-metal charge-transfer (LMCT) state might be responsible for the low quantum yield determined for $[EuL^1]^{3+}$. A density functional theory (DFT) study provides very similar energies for the ligand-centered excited singlet ($^1\pi\pi^*$) and triplet ($^3\pi\pi^*$) states of $[EuL^1]^{3+}$ and $[EuL^2]^{3+}$. The energy of the ^{9}LMCT state of $[EuL^1]^{3+}$ was estimated to be 20 760 cm^{-1} by using all-electron relativistic calculations based on the DKH2 approach, a value that decreases to 15 940 cm^{-1} upon geometry relaxation.

* l.charbonn@unistra.fr
† carlos.platas.iglesias@udc.es

Introduction

Luminescent lanthanide(iii) (Ln^{III}) complexes have received great attention in the last two decades due to their important applications in bioanalytical assays,[1] in cellulo studies[2] and optical imaging.[3] Most of this attention was devoted to complexes of Eu^{III} and Tb^{III}, which emit in the visible region of the spectrum and present long emission lifetimes in the ms range.[4] Complexes of these metal ions to be used as luminescent labels must meet a number of requirements including high stability in competitive biological media, a good protection from the environment to minimise vibrational quenching effects due to the presence of coordinated water molecules,[5] and the presence of chromophoric units to collect the excitation photons and transfer the energy from the ligand-centred excited state(s) to the excited state of the Ln^{III} ion.[6] Besides high luminescence quantum yields, Ln^{III} complexes for application as luminescent labels should be also endowed with high absorption coefficients at the excitation wavelength, resulting in bright probes.[7] Finally, long excitation wavelengths are also beneficial for biological applications, as they reduce phototoxicity in living systems and limit auto-fluorescence of biological samples.[8]

The vast majority of Ln^{III} luminescent complexes developed for application as optical probes in optical imaging or in cellulo studies are derivatives of cyclen.[4,9] This macrocyclic platform has the advantage of ensuring a high thermodynamic stability of the complexes.[10] Furthermore, the synthetic chemistry of cyclen is well developed, allowing for the introduction of different types and numbers of pendant arms at will.[11] However, other macrocyclic platforms such as tacn[12] or cryptands[13] were also shown to present advantageous properties for the development of Ln^{III}-based luminescent complexes.

The lanthanide complexes of the ligand L^1 (Scheme 1), which is based on a 18-membered macrocycle, were reported by some of us already in 2006.[14] The structure of the complexes both in the solid state and in solution was investigated in detail, showing the formation of 10-coordinate complexes in which the ten nitrogen atoms of the ligand coordinate to the Ln^{III} ions. More recently, we also explored the Ln^{III} complexes of the related ligand L^2, which were proposed as Magnetic Resonance Imaging (MRI) PARACEST contrast agents.[15,16] These complexes were found to be particularly inert with respect to their dissociation in strongly competitive media (1 M HCl). Given these interesting results, we decided to revisit the complexes of L^1, which contain up to six pyridyl chromophoric units in the ligand backbone. Herein we report the results of this study, which includes a detailed investigation of the photophysical properties of the Eu^{III} and Tb^{III} complexes. To rationalize the results of the photophysical study, we also performed cyclic voltammetry experiments and DFT calculations. These techniques provided support for the presence of a charge-transfer state of the Eu^{III} complex that quenches rather efficiently the metal-centred luminescence of $[EuL^1]^{3+}$.

Results and discussion

Synthesis of the complexes

The complexes of L^1 reported earlier were isolated as $[LnL^1][(Ln(NO_3)_6(H_2O)_x]$ salts, which contained $[(Ln(NO_3)_6(H_2O)_x]^{3-}$ anions.[14] The presence of the nitrate complex as counterion may be problematic for the characterisation of the complexes using certain techniques (*i.e.* cyclic voltammetry measurements). Thus, we prepared and isolated the Eu^{III}, Gd^{III} and Tb^{III} complexes of L^1 as simple nitrate salts with formula $[LnL^1](NO_3)_3 \cdot xH_2O$. Elemental analysis and mass spectral studies confirm the formation of the complexes (see Experimental section below). The ^1H NMR spectrum of the Eu^{III} complex recorded in D_2O solution presents 12 well-resolved signals (Fig. S1, ESI[i]), suggesting the presence of a single species in solution (within the detection limit of NMR) with an effective D_2 symmetry. The ^1H NMR spectrum recorded in d_3-MeOD at low temperature (193 K) is also in line with D_2 symmetry (Fig. S2, ESI[i]), with no evidence of fluxional behaviour being observed.

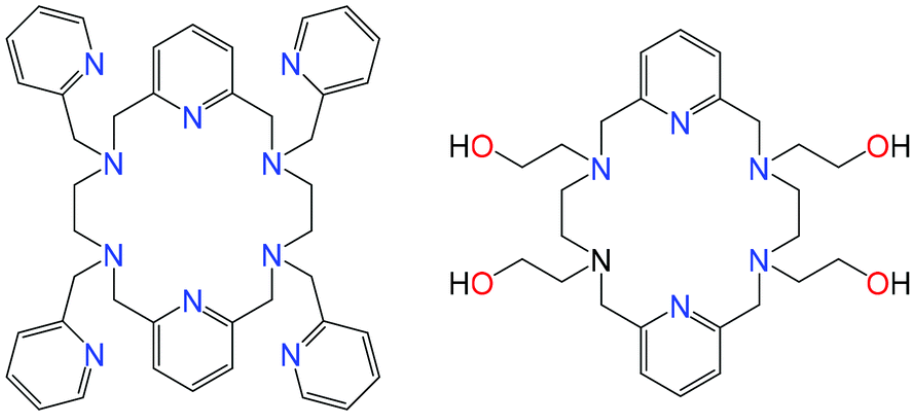

Scheme 1. Structures of the ligands discussed in this work.

Photophysical properties of the $[TbL^1]^{3+}$ complex

The UV-visible spectrum of $[TbL^1]^{3+}$ recorded in aqueous solution at pH = 7.0 is characterized by a strong absorption band centred at 266 nm (ε = 18 450 $M^{-1}cm^{-1}$), which accounts for the $\pi \rightarrow \pi^*$ transitions of the pyridyl rings. Exciting into this transition gave rise to the typical emission pattern characteristic of the $^5D_4 \rightarrow {}^7F_J$ (J = 6–3) transitions of the Tb^{III} ion (Fig. 1).[1b] As expected, the excitation spectrum recorded upon metal-centred emission is very similar to the corresponding absorption spectrum, as a result of the antenna effect.

The luminescence decay profiles of the $[TbL^1]^{3+}$ complex could be perfectly fitted to mono-exponential decays with lifetimes in water and deuterated water of τ_{H2O} = 3.27 ms and τ_{D2O} = 4.08 ms, which are indicative of the absence of water molecules in the first coordination sphere.[17] Despite these long lifetimes, quantum yields are rather low and values of ϕ_{H2O} = 7.4 and ϕ_{D2O} = 8.9% have been measured at pH = 7.0 and pD = 7.3, respectively, using Rhodamine 6G in aerated water as a reference (ϕ = 0.76).[18] Although low, these low quantum yields are in agreement with literature data for pyridyl-based Tb^{III} complexes.[19]

Photophysical properties of the $[EuL^1]^{3+}$ complex

When recorded in H_2O, the high resolution emission spectrum of $[EuL^1]^{3+}$ (Fig. 1) indicates the presence of a major species, with a very faint emission of the $^5D_0 \rightarrow {}^7F_0$ transition around 579.5 nm and with three main components centred at 582.5, 592.4 nm and 595.5 nm, respectively, accounting for the three sublevels of the $^5D_0 \rightarrow {}^7F_1$ transitions expected in the case of a complex with low symmetry.[1b] Sensitized emission quantum yields of less than 1% have been measured in H_2O and in D_2O by comparison with $[Ru(bpy)_3]Cl_2$ as a reference[20] (Table 1), showing that this species is weakly luminescent. Interestingly, one can also notice the presence of weak emission peaks, which increased in D_2O solution, at 585.5, 590.5 and 597.6 nm, indicative of a second species in solution (Fig. 2). A remarkable feature of this emission spectrum is the high relative intensity of the $^5D_0 \rightarrow {}^7F_4$ transition observed at *ca.* 684 nm. Also worthy of interest, the $^5D_0 \rightarrow {}^7F_{5,6}$ transitions centered around 747 and 825 nm could be easily observed, amounting to *ca.* 6(1)% and 12(1)% of the total intensity. Considering that the instrumental response of the conventional red photomultiplier (PM, Hamamatsu R928) is generally important in this spectral region, the spectrum was also recorded with a NIR sensitive PM (Hamamatsu R5509-72), confirming the previous results. The observation of the $^5D_0 \rightarrow {}^7F_{5,6}$ transitions is rather rare,[21] and must be related to the particular symmetry of

the crystal field around the Eu^{III} cation. The X-ray structures of the La^{III} and Tm^{III} complexes evidenced a bicapped square antiprismatic coordination polyhedron. DFT calculations performed on the $[EuL^1]^{3+}$ complex point to a D_2 symmetry of the complex and confirm the bicapped square antiprismatic coordination polyhedron (see DFT study below). This provides a coordination polyhedron with a distorted D_{4d} symmetry. In D_{4d} symmetry the $^5D_0 \rightarrow {}^7F_2$ transition is symmetry forbidden, while the $^5D_0 \rightarrow {}^7F_4$ transition is intense due to the absence of an inversion centred. This explains the very intense $^5D_0 \rightarrow {}^7F_4$ transition compared to the $^5D_0 \rightarrow {}^7F_2$ one in $[EuL^1]^{3+}$, a situation that is also commonly observed for Eu^{III} DOTA derivatives showing capped square antiprismatic coordination.[22] The relatively high intensity of the $^5D_0 \rightarrow {}^7F_{5,6}$ transitions appears to be also related to the distorted D_{4d} symmetry of the coordination polyhedron (see below). The asymmetry ratio, *R*, defined as the ratio between the forced electric dipole $^5D_0 \rightarrow {}^7F_2$ and the magnetic dipole $^5D_0 \rightarrow {}^7F_1$ transitions,[23] was determined to be 0.93, which is in agreement with spectra observed for other Eu complexes with D_{4d} symmetry.[24]

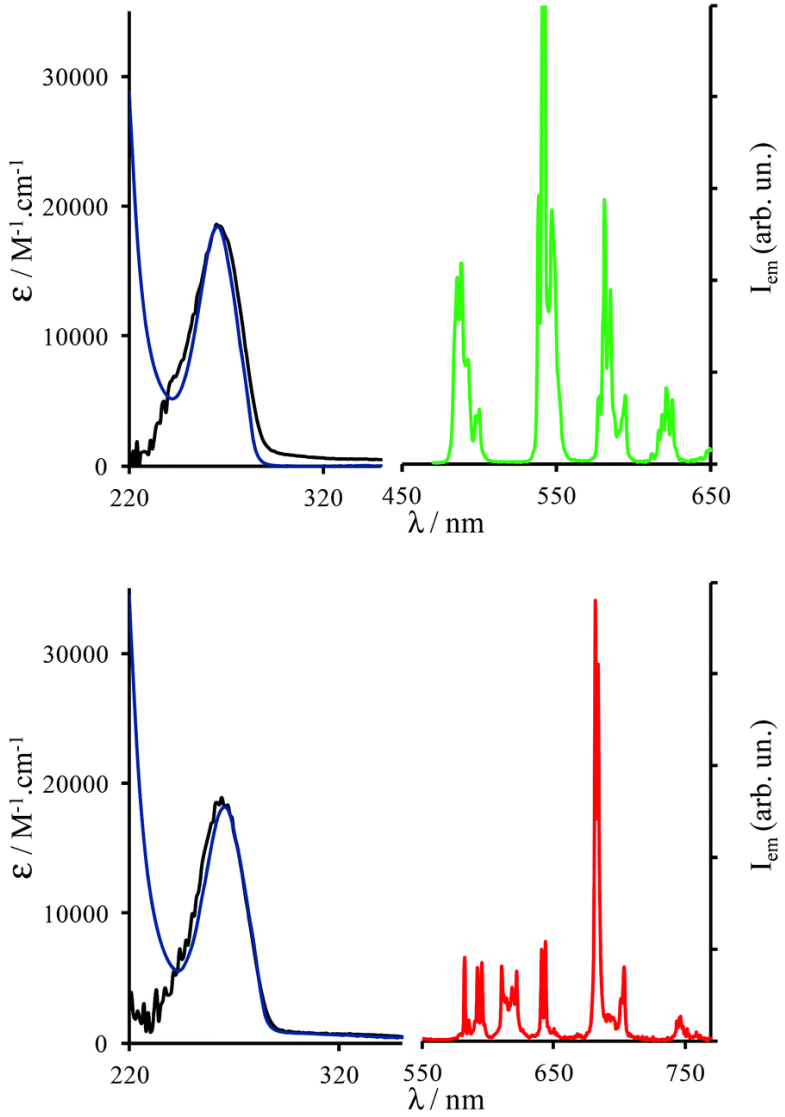

Fig. 1. UV/Vis absorption spectra (blue), excitation spectra (black, Ln = Eu, λ_{em} = 610.5 nm; Ln = Tb, λ_{em} = 545 nm) and high resolution emission spectra (λ_{exc} = 265 nm) recorded in aqueous solution at r.t for the ($[LnL^1]^{3+}$) complexes (top: Ln = Tb, pH = 7.0, 9.1×10^{-5} M, green; bottom: Ln = Eu, pH = 7.0, 8.8×10^{-5} M, red).

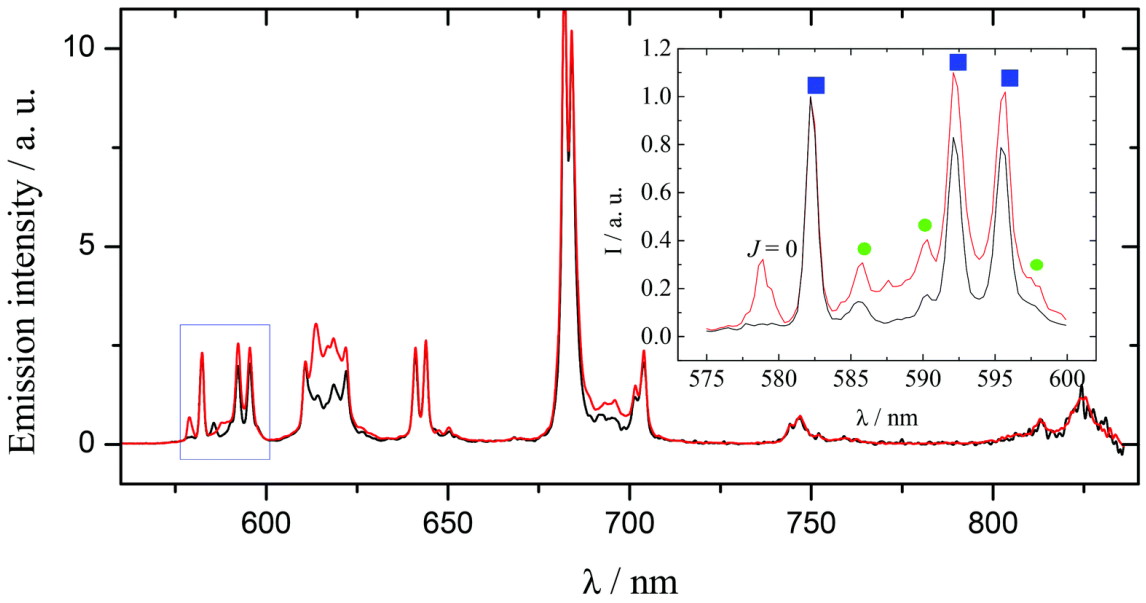

Fig. 2. High resolution emission spectra (λ_{exc} = 265 nm, emission slits = 0.3 nm, 2 pt nm^{-1}) recorded for [EuL^1]$^{3+}$ in H_2O (black, 8.8 × 10^{-5} M, pH = 7.0) and in D_2O (red, 9.0 × 10^{-5} M, pD = 7.3), normalized at 582 nm. Inset: Zoom of the $^5D_0 \rightarrow {}^7F_0$ and $^5D_0 \rightarrow {}^7F_1$ emission bands in the same conditions (except for an increment of 10 pt nm^{-1}), showing the signature of the two species (■ and ●), see text.

Table 1. Selected photophysical data for [LnL^1]$^{3+}$ and [LnL^2]$^{3+}$ complexes (Ln = Eu, Tb) in aqueous solutions, pH = 7.0 in H_2O and pD = 7.3 in D_2O, r.t. λ_{exc} = 265 nm[a].

Ln	ε (M^{-1}cm^{-1})/λ (nm)	ϕ_{H2O} (%)	ϕ_{D2O} (%)	τ_{H2O} (ms)	τ_{D2O} (ms)	q[b]
[EuL^1]$^{3+}$	18 200/265	0.10	0.24	τ_1 = 1.4	τ_1 = 2.11	0.0
				τ_2 = 0.47	τ_2 = 1.30	1.3
[EuL^2]$^{3+}$	7900/270	1.6	5.3	0.49	1.36	See text
[TbL^1]$^{3+}$	18 500/266	7.4	8.9	3.27	4.08	0.0
[TbL^2]$^{3+}$	8800 /268	21.0	40.6	2.12	3.87	

[a] Estimated errors: ±10% on lifetimes, ±15% on quantum yields. [b] According to ref. 17.

Table 2. Lifetimes of [EuL^1]$^{3+}$ in H_2O (8.8 × 10^{-5}M, pH = 7.0) at various emission wavelengths (r.t, λ_{exc} = 265 nm).

λ_{em}/nm	τ_1 (ms)/B_1[a] (%)	τ_2 (ms)/B_2[a] (%)
582	1.409(2)/9	0.403(1)/91
610.5	1.47(7)/25	0.478(3)/75
682	1.3(1)/9	0.404(1)/91

[a] B_i are the normalized pre-exponential factors (B_1 + B_2 = 100) obtained from the fit of the emission decay curves to a bi-exponential model.

The luminescence decay profiles recorded at various emission wavelengths did not give strictly mono-exponential decay profiles (Table 2), confirming the presence of the second species in solution with contributions varying from 9 to 25% in H_2O depending on the emission wavelengths. The strong difference between the values of the measured lifetimes probably arises from the presence of a mono-hydrated species (with $\tau_2 \sim 0.43$ ms) and a non-hydrated species (with $\tau_1 \sim 1.4$ ms).

Another striking result was observed when H_2O was replaced by D_2O. As seen in Fig. 2, significant changes in the shape of the emission spectrum of the Eu^{III} complex were observed, which also strongly supports the presence of two species with different hydration states in solution.[25] Due to the reduction of vibrational quenching in D_2O, several transitions are increased and more particularly the $^5D_0 \rightarrow {}^7F_2$ transition at 610.5 nm and the $^5D_0 \rightarrow {}^7F_0$ transitions centred around 578.9 nm. On the latest, high resolution was performed and the corresponding spectrum is depicted in Fig. 3.

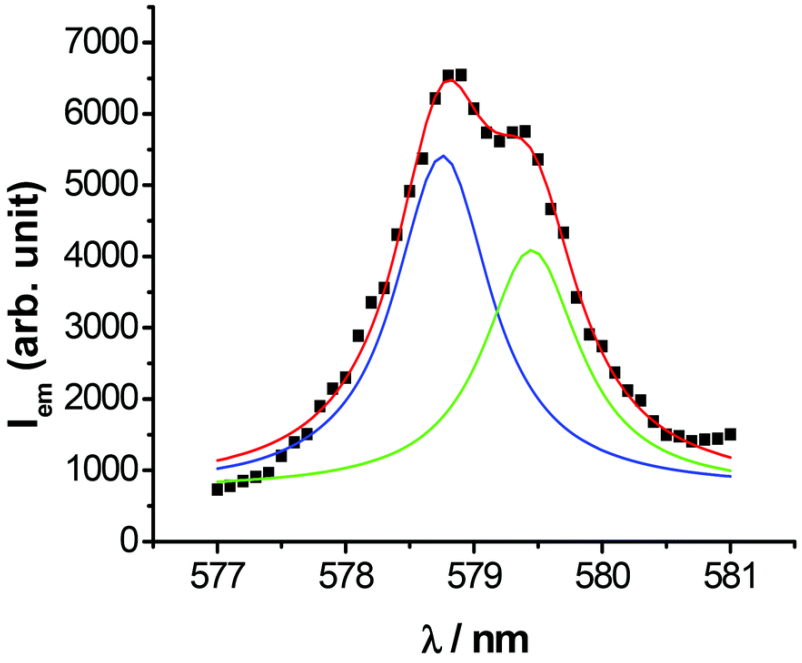

Fig. 3. The high resolution emission spectrum of $[EuL^1]^{3+}$ (D_2O, λ_{exc} = 265 nm) of the $^5D_0 \rightarrow {}^7F_0$ region showing the experimental points (■), the fitting to the sum of two Lorentzian peaks (—) and the individual Lorentzian contributions (—, —).

The spectrum of Fig. 3 could be deconvoluted as a sum of two Lorentzian curves (R^2 = 0.983) with maxima at 578.8 nm and 579.4 nm, respectively. Time-resolved decay measurements were registered at various specific wavelengths of this transition (with narrow emission slits of 0.2 nm) and the data were fitted to bi-exponential decay functions with a fixed long lifetime parameter of τ_1 = 2.11 ms, while the shorter lifetime, τ_2, and the two pre-exponential factors were varied. Single exponential decays corresponding with τ_1 = 2.11 ms were observed in the 578.0–578.2 nm region. Between 578.3 and 580.5 nm, all decays could be fitted with τ_2 values ranging from 1.28 to 1.37 ms. Variations of the respective pre-exponential factors (B_i) are represented in Fig. S3 (ESI[i]) and are in agreement with the formation of the two species identified by the peak analysis. The shorter value of τ_2 and the hyperchromicity of this peculiar transition in D_2O is in agreement with a $[EuL^1(D_2O)]^{3+}$ species, in which a pyridine ring would be decoordinated, leaving the space for a water molecule in the first coordination sphere. We thus assumed that τ_1 accounts for a species with q = 0 and bicapped square-antiprismatic geometry.[21] These hypothesis is in agreement with the hydration numbers calculated for the two species from the equation of Beeby *et al.* (see Table 1).[17]

The presence of two complex species in solution is in sharp contrast with the simple ^{1}H NMR spectrum recorded in D_2O solution (Fig. S1, ESI[i]). Given the different concentration ranges typically used for luminescence (μM) and NMR (mM) measurements, we recorded luminescence measurements in more concentrated solutions upon selective excitation into the f–f absorption bands at 395, 399 or 412 nm (Fig. S4, ESI[i]). These spectra were virtually identical with a single transition for the $^5D_0 \rightarrow {}^7F_0$ band at 582 nm and two components for the $^5D_0 \rightarrow {}^7F_1$ transition. The $^5D_0 \rightarrow {}^7F_2$ massive is weakly emitting, whereas the transitions to $^7F_3$ and $^7F_4$ are surprisingly intense. When exciting at high energy (300 nm), new bands could be observed in the spectrum at 578.0 and 584.5 nm, around 616 nm and in the 690–700 nm region. Interestingly, the appearance of these new bands is in agreement with the results obtained when measuring the samples at lower concentration (9×10^{-5} M, λ_{exc} = 265 nm) changing the solvent from H_2O to D_2O (Fig. S4, ESI[i]).

The presence of two species in solution evidenced by the photophysical study of $[EuL^1]^{3+}$ is rather surprising considering the presence of a single species in solution with an effective D_2 symmetry observed by NMR. Given the very low emission quantum yield of $[EuL^1]^{3+}$ (0.1%), we attribute the second (minor) species present in solution to a complex presenting a much higher emission quantum yield, so that it provides a sizeable contribution to the overall emission spectrum in spite of its low concentration (below the detection limit of NMR). This species could be for instance a nine-coordinated complex in which one of the pendant arms is not bound to the metal ion. Such nine-coordinate species were found to be the major species in solution for complexes with the small Ln^{III} ions based on the same 18-membered macrocycle and containing acetate pendant arms.[26]

Photophysical properties of the $[LnL^2]^{3+}$ complexes (Ln = Eu and Tb)

The photophysical properties of the previously reported $[LnL^2]^{3+}$ complexes were investigated to gain insight into the peculiar behaviour of the corresponding complexes of L^1. The UV-visible spectra of the two complexes in aqueous solutions at pH = 7.0 are characterized by a strong absorption band centred at 266–268 nm, which accounts for the $\pi \rightarrow \pi^*$ transitions of the pyridyl rings (Table 1). Exciting into these transitions gave rise to the typical emission patterns characteristic of the $^5D_0 \rightarrow {}^7F_J$ (J = 0–4) and $^5D_4 \rightarrow {}^7F_J$ (J = 6–3) transitions of the Eu^{III} and Tb^{III} ions, respectively (Fig. S4 and S5, ESI[i]). As expected, the excitation spectra recorded upon metal-centred emission are very similar to the corresponding absorption spectra, as a result of the antenna effect.

As previously observed for the L^1 analogue (see above), the emission spectrum of $[EuL^2]^{3+}$ displays a very peculiar pattern. In particular, the $^5D_0 \rightarrow {}^7F_4$ transition is very intense with a maximum at 683 nm and is only weakly degenerated with two main transitions (Fig. S5, ESI[i]). The luminescence decay profiles of the Eu^{III} complex could be perfectly fitted to mono-exponential decays to give the following lifetimes: τ_{H2O} = 0.49 ms in water and τ_{D2O} = 1.36 ms in deuterated water. The luminescence decay profiles of the Tb^{III} complex could also be fitted to mono-exponential decays to yielding τ_{H2O} = 2.12 ms in water and τ_{D2O} = 3.78 ms in deuterated water. The much longer emission lifetimes determined in D_2O solution reflect the quenching effect of the O–H oscillators of the four coordinated alcohol groups. The structure of the $[EuL^2]^{3+}$ complex in solution is similar to that of $[EuL^1]^{3+}$, with four O–H oscillators of the alcohol groups of the pendant arms being directly coordinated to the metal ion.[15,16] The use of Beeby's method to compute the number of coordinated O–H oscillators,[17] assuming that each coordinated alcohol group provides a quenching effect equal to half of that provided by a water molecule, provides values of 2.6 and 1.6 oscillators for the Eu^{III} and Tb^{III} complexes, respectively. Since four O–H oscillators are coordinated to the metal ion and that mono-exponential decays are measured, one can assume that the quenching results from the oscillators of the hydroxyethyl groups (with an estimated k_{OH} = 325 s^{-1} for Eu and k_{OH} = 52 s^{-1} for Tb) hence providing a quenching effect that is lower than those of coordinated water molecules.

In contrast to $[EuL^1]^{3+}$, the high resolution emission spectra of $[EuL^2]^{3+}$ indicates the presence of a single species with a very faint emission of the $^5D_0 \rightarrow {}^7F_0$ transition around 579 nm, in accordance with the mono-exponential decay. The quantum yields have also been calculated with values of Φ_{H2O} = 1.6% and Φ_{D2O} = 5.4% (at pH = 7.0 and pD = 7.4, respectively, using $[Ru(bipy)_3]Cl_2$ in aerated water as a reference (Φ = 4%)).[20] The quantum yields are *ca.* 20 times higher than those determined for $[EuL^1]^{3+}$ (Table 1). The quantum yields of the Tb^{III} complex have also been calculated with values of Φ_{H2O} = 21.0% and Φ_{D2O} = 40.7% (at pH = 7.0 and pD = 7.4, respectively). These values also represent an important improvement with respect to the L^1 analogue, but the effect is far less important than in the case of the Eu^{III} complexes. The higher quantum yields determined for $[TbL^2]^{3+}$ compared to $[TbL^1]^{3+}$ suggest different efficiencies of the energy transfer from the pyridyl units of the ligand. This energy transfer is likely more efficient when involving the pyridyl units of the macrocycle, which are tightly bound to the metal ion, than in the case of the pyridyl pendant arms, as the latter are characterized by considerably longer Ln–N distances (Table 3). Thus, four of the six pyridyl chromophores of $[EuL^1]^{3+}$ would be less efficient in transferring their energy to the metal ion than the two pyridyl units of the macrocycle.

Table 3. Calculated bond distances (Å) of the Eu coordination environments obtained for $[EuL^1]^{3+}$ and $[EuL^2]^{3+}$ using 46 + $4f^6$ and 46 + $4f^7$ core definitions[a]

	Core	Eu–N_{am}	Eu–N_{py}	Eu–N_{arm}	Eu–O
$[EuL^1]^{3+}$	46 + $4f^6$	2.702	2.598	2.829	—
$[EuL^1]^{3+}$ [b]	46 + $4f^7$	2.718	2.675	2.795	—
		2.812	2.742	2.885	
		3.006		3.153	
		4.320		5.998	
$[EuL^2]^{3+}$	46 + $4f^6$	2.689	2.590	—	2.556
$[EuL^2]^{3+}$ [b]	46 + $4f^7$	2.692	2.609	—	2.735
		2.729	2.677		2.779
		2.836			2.835
		3.447			2.884

[a] N_{am}, N_{Py} and N_{arm} denote amine nitrogen atoms, pyridyl nitrogen atoms of the macrocycle and nitrogen atoms of the pyridyl pendants, respectively. [b] Spin-unrestricted calculations using a pseudo-doublet configuration.

Cyclic voltammetry experiments

The very low emission quantum yield of $[EuL^1]^{3+}$ might be related to the presence of a ligand-to-metal charge-transfer (LMCT) state. Indeed, low lying LMCT states are known to quench rather efficiently the Eu^{III} luminescence, as proposed for instance for Eu^{III} acetylacetonates,[27] complexes with tridentate aromatic units[28] containing nitrogen donor atoms or calixarene complexes.[29] However, with some exceptions,[29] LMCT states are usually not directly observed in the absorption spectra of complexes with aromatic units, being hidden by the much more intense $\pi \rightarrow \pi^*$ absorption bands.[28] These LMCT transitions are the result of an electron transfer process in which the Eu^{III} ion is formally reduced to Eu^{II}. Thus, cyclic voltammetry experiments were carried out in aqueous 0.1 M KCl to assess the ability of L^1 to stabilize divalent Eu.

The CV curves (Fig. 4) are typical of a reversible system with a half-wave potential of −620 mV and a difference between the anodic and cathodic waves of ΔE = 64 mV. This indicates that the divalent Eu

complex is stable under the conditions used for cyclic voltammetry experiments. In contrast, the cyclic voltammogram of the $[EuL^2]^{3+}$ complex (Fig. S7, ESI[i]) presents a reduction peak at more negative potential (−1040 mV) with respect to $[EuL^1]^{3+}$ (−652 mV), showing that replacing the pyridyl pendant arms of L^1 by harder hydroxyethyl donors is unfavourable for the stabilization of Eu^{II}. The reverse scan of $[EuL^2]^{3+}$ shows an anodic peak in the range −560 to −610 mV depending on the scan rate. Thus, the cyclic voltammogram of $[EuL^2]^{3+}$ is characteristic of an irreversible system. In the case of $[EuL^1]^{3+}$ both the anodic and cathodic peak currents show a linear relationship with the square root of the scan rate, which points to a diffusion controlled process (Fig. S8, ESI[i]).

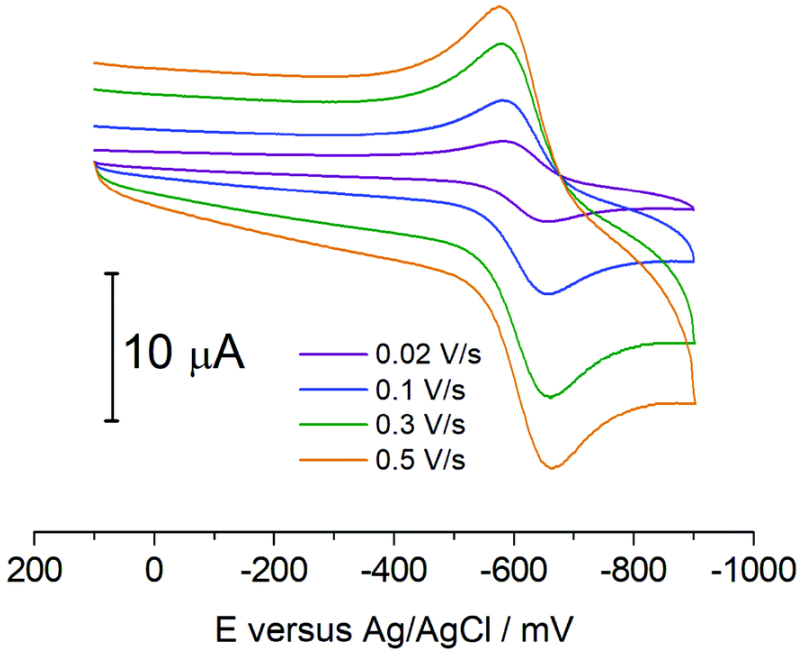

Fig. 4. Cyclic voltammograms of $[EuL^1]^{3+}$ recorded from a 1 mM aqueous solution (0.1 M KCl, pH 7.0) at varying scan rates.

The CV curves obtained for $[EuL^1]^{3+}$ and $[EuL^2]^{3+}$ highlight the effect that the presence of softer donor atoms in the ligand scaffold has on the stabilization of divalent Eu. A similar effect was observed previously by replacing oxygen atoms of cryptands by softer S donor atoms,[30] or harder negatively charged carboxylate donors by neutral amides.[31] Furthermore, the relatively large cavity of the macrocyclic fragment of L^1 also contributes to the stabilization of divalent Eu^{II}.[31] Nevertheless, the $[EuL^1]^{3+}$ complex still possesses a lower stability against oxidation than the aquated ion,[32] for which a half-wave potential of −585 mV was reported (−620 mV for $[EuL^1]^{3+}$).

Computational study

Aiming to find additional support for the presence of a LMCT state that quenches the Eu^{III}-centred emission of $[EuL^1]^{3+}$ we carried out a computational DFT study. Geometry optimizations of the $[EuL^1]^{3+}$ and $[EuL^2]^{3+}$ systems were carried out at the TPSSh/LCRECP/6-31G(d,p) level following the methodology described before[33] (see also computational details below). These calculations employed the large-core approximation, which includes the 4f electrons in the core, and were thus carried out with the spin-restricted formalism. The optimized geometries of the complexes provide molecular geometries very similar to those reported previously on the basis of both X-ray diffraction studies and DFT calculations.[14] For $[EuL^1]^{3+}$, the Eu–N distances involving donor atoms of the pendant arms (2.829 Å, Table 3) are longer than those to the

pyridyl donor atoms of the macrocycle (2.598 Å), while the bond distances involving amine nitrogen atoms take an intermediate value (2.702 Å). The coordination polyhedron (Fig. 5) can be described as a bicapped square antiprism, where two nitrogen atoms of the pendant arms and two amine nitrogen define the square faces of the polyhedron (rms deviation 0.152 Å). The mean twist angle of the two square faces (48°) is very close to that expected for a square antiprism (45°). The nitrogen atoms of the two remaining dangling pyridyl units of the macrocycle are each capping one of the square faces.

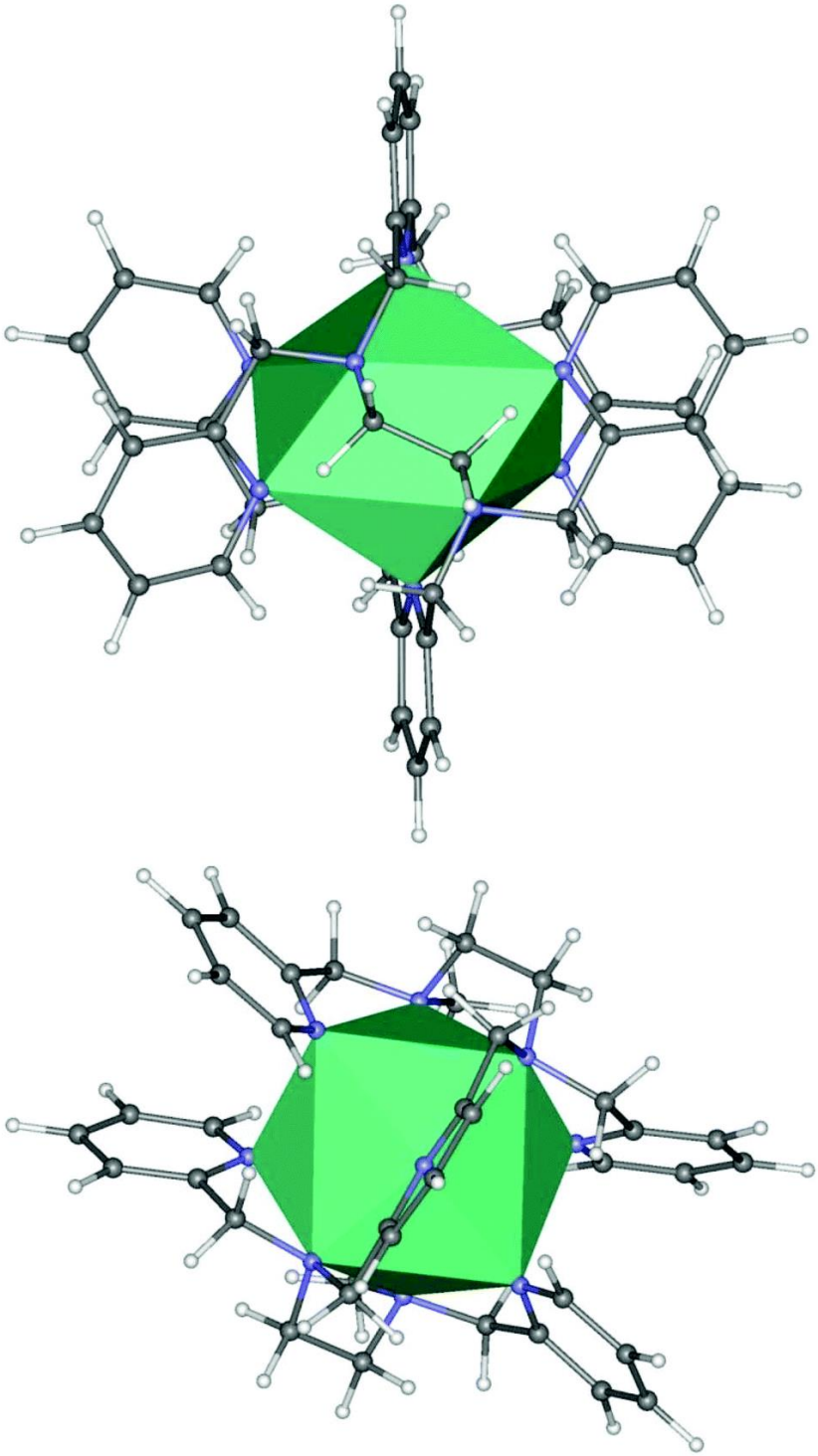

Fig. 5. Two views of the bicapped square antiprismatic coordination polyhedron in $[EuL^1]^{3+}$. The geometry of the complex was obtained with DFT calculations.

DFT calculations were also used to estimate the energies of the lowest-energy ligand-centred triplet states of $[EuL^1]^{3+}$ and $[EuL^2]^{3+}$. For this purpose the triplet states were optimized at the TPSSh/LCRECP/6-31G(d,p) level and their energies with respect to the singlet ground state were obtained (ΔSCF method).[34] Thus, the energies of the lowest-energy excited triplet states include the relaxation effects in the triplet excited states. The results (Table 4) indicate that the energies of the lowest-energy $^3\pi\pi^*$ states of $[EuL^1]^{3+}$ and $[EuL^2]^{3+}$ are virtually identical (~28 610 cm^{-1}). Furthermore, the low energy triplet state was estimated from the low temperature luminescence spectrum of the parent $[GdL^1]^{3+}$ complex (Fig. S16[i]). The intercept between the slope of the high energy tail of the emission spectrum and the energy axis led to a triplet state at 26 810 cm^{-1}, slightly lower than the calculated one. The values calculated for the energies of the $^3\pi\pi^*$ states are in excellent agreement with the experimental value determined for DO3A derivatives containing pyridyl pendant arms (28 500 cm^{-1}).[35] Thus, the results shown in Table 4 indicate that the energies of the ligand-centred lowest-energy $^3\pi\pi^*$ and $^1\pi\pi^*$ states do not explain the very different emission quantum yields of the complexes with L^1 and L^2.

Table 4. Energies of the ligand-centered singlet ($^1\pi\pi^*$) and triplet ($^3\pi\pi^*$) excited states and the excited ligand-to-metal charge transfer states (^{9}LMCT) of $[EuL^1]^{3+}$and $[EuL^2]^{3+}$ obtained with DFT calculations. All values are in cm^{-1}.

	$[EuL^1]^{3+}$	$[EuL^2]^{3+}$
$^1\pi\pi^*$[a]	36 526	38 225
$^3\pi\pi^*$ [b]	28 609	28 619
^{9}LMCT [c]	20 763	22 537
^{9}LMCT [d]	15 937	16 728

[a] Obtained with TDDFT calculations and the LCRECP approach. [b] Obtained with ΔSCF calculations and the LCRECP approach. [c] Obtained with ΔSCF calculations (DKH2 approach) using the ground-state geometry. [d] Obtained with ΔSCF calculations (DKH2 approach) using the relaxed excited-state geometry (see text).

Geometry optimization of the $[EuL^1]^{3+}$ complex was followed by the calculation of the excited singlet states using TDDFT calculations. The absorption profiles obtained from these calculations are in reasonably good agreement with the experimental ones. The absorption maxima calculated with TDDFT are 251 and 241 nm for $[EuL^1]^{3+}$ and $[EuL^2]^{3+}$, respectively. The energies of the ligand-centred excited singlet states with the lowest energy are given in Table 4.

The modelling of the LMCT states of $[EuL^1]^{3+}$ and $[EuL^2]^{3+}$ was found to be more challenging. We initially attempted TDDFT calculations on the septet ground state of $[EuL^1]^{3+}$ using a SCRECP, which includes the 4f electrons in the valence space.[36] Unfortunately, these calculations did not achieve convergence because of the presence of many low-lying excited states. We then focused our attention on the ^{9}LMCT state, which should correspond to a system with a Eu $4f^7$ sub-configuration. All-electron relativistic calculations based on the DKH2 approach (see computational details below) were therefore performed to obtain the expected septet ground state, in which the alpha LUMO corresponded to one of the Eu 4f orbitals. The alpha HOMO, which does not have significant Eu 4f contribution, and the alpha LUMO, were then rotated. The subsequent SCF calculation converged to the desired ^{9}CT state, in which all Eu 4f orbitals are occupied.

The analysis of the charges and spin-density values of the Eu atom, obtained with Mulliken population analysis, confirm that our calculations converged to the excited ^{9}LMCT state (Table 5). The excited ^{9}LMCT states of both $[EuL^1]^{3+}$and $[EuL^2]^{3+}$ are characterised by a lower atomic charge on Eu, as would be expected. The total spin population of the ground state (~6.3) is in line with the expected $4f^6$ configuration, being very similar to those reported for other Eu^{III} complexes.[37] The excited ^{9}LMCT state is characterized by a higher spin population on the Eu atom (~7.0), which is characteristic of systems with a $4f^7$ configuration such as Gd^{III} complexes.[38] Most of the spin population on the Eu atom resides on the 4f orbitals, with smaller contribution from s, p and d orbitals.

Table 5. *s*, *p*, *d*, and *f* spin populations and atomic charges (*Q*) on the Eu atom calculated with relativistic DKH2 calculations for the septet ground state and the excited ^{9}LMCT state of $[EuL^1]^{3+}$ and $[EuL^2]^{3+}$.

	s	*p*	d	*f*	Total	*Q*
$[EuL^1]^{3+}$ [a]	0.03	0.04	0.09	6.12	6.28	+2.35
$[EuL^1]^{3+}$ [b]	0.03	0.04	0.07	6.89	7.04	+1.51
$[EuL^2]^{3+}$ [a]	0.02	0.03	0.08	6.11	6.25	+2.10
$[EuL^2]^{3+}$ [b]	0.03	0.05	0.08	6.87	7.03	+1.60

[a] Ground state. [b] ^{9}LMCT state.

The excited ^{9}LMCT state of $[EuL^1]^{3+}$ is calculated to lie 20 760 cm^{-1} above the ground state, an energy that is close to that of the excited $^5D_0$ of Eu (17 256 cm^{-1}). It is worth noting that the energy of the excited ^{9}LMCT state was calculated using the ground state geometry, and therefore corresponds to a vertical energy. These calculations therefore confirm the presence of an excited ^{9}LMCT state for $[EuL^1]^{3+}$ whose energy is likely comparable to that of the excited $^5D_0$ level of Eu. The presence of this low-lying ^{9}LMCT state is possibly responsible for the non-radiative deactivation of the Eu $^5D_0$ state, which results in a very weak Eu^{III}-centred emission. The harder nature of the oxygen donor atoms in $[EuL^2]^{3+}$ results in a somewhat higher energy of the ^{9}LMCT state (22 537 cm^{-1}), which is therefore likely more difficult to access by thermal population from the excited Eu $^5D_0$ state.

We next decided to assess the effects of geometry relaxation in the excited ^{9}LMCT states of both $[EuL^1]^{3+}$ and $[EuL^2]^{3+}$. For that purpose we performed geometry optimizations of these systems within the spin-unrestricted formalism using a pseudo-doublet configuration and a large-core quasi-relativistic pseudopotential that incorporates 46 + $4f^7$ electrons in the core for Eu. These optimized geometries present Eu-donor distances that are considerably longer than those obtained with the small core that includes 46 + $4f^6$ electrons in the core, as would be expected considering that larger ionic radius of Eu^{II} compared to Eu^{III}. The calculated bond distances are shown in Table 3. Noteworthy, the optimised geometries obtained with the 46 + $4f^7$ pseudopotential are very distorted, in contrast with the D_2 symmetry obtained for the ground state. For $[EuL^1]^{3+}$, two of the amine nitrogen atoms and two nitrogen atoms of the pendant arms are either not involved in coordination to the metal ion or provide a very weak interaction (Table 3). In the case of $[EuL^2]^{3+}$, one of the amine nitrogen atoms is not involved in coordination to the metal ion (Eu–N = 3.447 Å, Table 3). We therefore conclude that relaxed geometries of the excited ^{9}LMCT states present a considerable distortion with respect to the ground state. The energies of the excited ^{9}LMCT states were subsequently calculated using the relaxed geometries. The corresponding energies of the relaxed ^{9}LMCT states are considerably lower, falling below the energy of the Eu($^5D_0$) state (Table 4). Geometry relaxation

lowers more significantly the energy of the ^{9}LMCT state of $[EuL^{2}]^{3+}$, likely because of the more flexible nature of the pendant arms.

Fig. 6 illustrates the mechanism proposed for the non-radiative deactivation of the excited Eu($^{5}D_{0}$) state in $[EuL^{1}]^{3+}$. Similar pathways were proposed previously by Berry for a Eu^{III} tris(acetylacetonate) complex,[27] and by Sabbatini for the $Eu^{III} \subset$ 2.2.1 cryptate.[39] The Eu($^{5}D_{0}$) state presents a crossover to a low-lying LMCT state, which can be populated overcoming a thermal barrier. The potential of the LMCT state is shifted along the nuclear coordinate, as a consequence of the large distortion of the complex geometry on going from the Eu($^{5}D_{0}$) to the LMCT state, as evidenced by the bond distances compiled in Table 3. The LMCT state can subsequently experience an efficient relaxation to the $^{7}F_{J}$ states as a result of the large displacement of the two potentials. An alternative mechanism that could contribute to the low emission quantum yield of $[EuL^{1}]^{3+}$ would involve an electron transfer from the ligand-centred excited singlet and/or triplet states to the Eu^{III} ion, prior the formation of the $^{5}D_{0}$ state of Eu.[40]

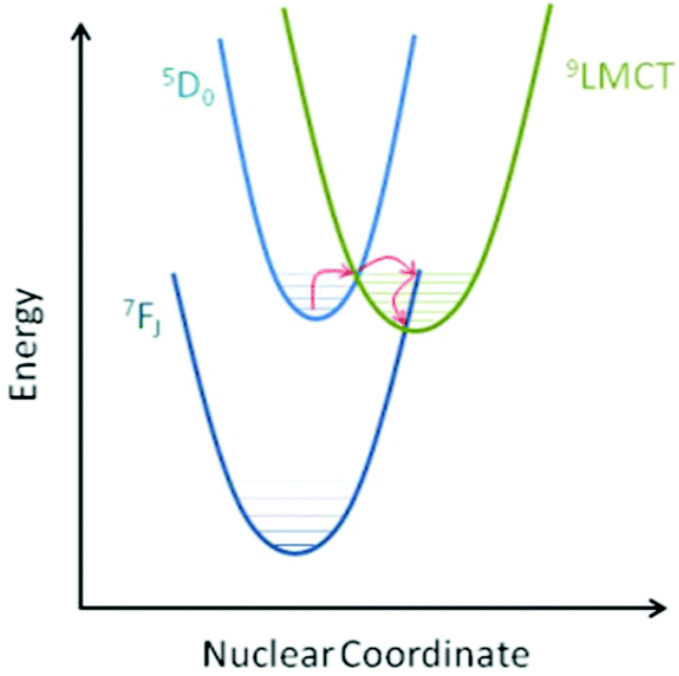

Fig. 6. Schematic representation of the non-radiative deactivation of the Eu($^{5}D_{0}$) state through a low-lying LMCT state.

Conclusions

A detailed photophysical study of the $[LnL^{1}]^{3+}$ and $[LnL^{2}]^{3+}$ complexes revealed some interesting features. The luminescence quantum yields of the Tb^{III} complexes are moderately high, particularly in the case of $[TbL^{2}]^{3+}$ (ϕ_{H2O} = 21%). The emission spectra of the $[EuL^{1}]^{3+}$ complex shows rather intense $^{5}D_{0} \rightarrow {}^{7}F_{5,6}$ transitions, which are often extremely weak. This has been related to the bicapped square antiprismatic coordination around the Eu^{III} ion, which results in a crystal field symmetry approaching D_{4d}. The emission quantum yield of $[EuL^{2}]^{3+}$(ϕ_{H2O} = 1.6%) is low, but this is expected because of the presence of four coordinated OH oscillators from the hydroxyethyl pendant arms. The emission quantum yield of $[EuL^{1}]^{3+}$is ~16 times lower, which is surprising considering the good protection of the Eu^{III} coordination environment offered by the ligand. The weak emission of $[EuL^{1}]^{3+}$ allowed us to detect a second emissive species in

solution, which is below the detection limit of NMR. The nature of this second species is not clear at this point, but it could be related to a form of the complex in which one of the pendant arms remains uncoordinated.

The low emission quantum yield of $[EuL^1]^{3+}$ prompted us to perform a cyclic voltammetry study, which showed that L^1 stabilises divalent Eu rather well compared to L^2. These results suggested that the presence of a LMCT state could be responsible for the weak emission observed for $[EuL^1]^{3+}$. Indeed, the results obtained with DFT calculations are consistent with the presence of a low-lying LMCT state in $[EuL^1]^{3+}$ whose energy is close to that of the Eu($^5D_0$) state. The energy of the corresponding LMCT state in $[EuL^2]^{3+}$ is ~2000 cm^{-1} higher according to our DFT results, which is in line with the more pronounced stabilization of divalent Eu by L^1 as a consequence of the softer nature of the donor atoms of the pendant arms. The results reported in this work have profound implication for the development of Eu^{III}-based luminescence materials.

Experimental section

Materials

The syntheses of compounds $[EuL^2](NO_3)_3\cdot 3H_2O$ and $[TbL^2](NO_3)_3\cdot 5H_2O$ was described previously.[15] Macrocycle L^1 was synthesised following the literature procedure.[14] All other chemicals purchased from commercial sources were of the highest available purity and were not purified further. Hydrated lanthanide(iii) nitrates were obtained from Aldrich. Solvents used were of reagent grade and purified by usual methods.

Measurements

Elemental analyses were performed in a Carlo-Erba EA 1108 microanalyser. Attenuated total reflection infrared (ATR-FTIR) spectra were recorded on a FP-6100 Jasco spectrometer. Electrospray-ionization (ESI) mass spectra were recorded on amicroTOF (focus) mass spectrometer (Bruker Daltonics, Bremen, Germany). Ions were generated using an ApolloII (ESI) source and ionization was achieved by electrospray. ^1H, NMR spectra were recorded in D_2O solutions (pD = 7.0) on a Bruker ARX400 NMR spectrometer (9.4 T).

Cyclic voltammograms were recorded using a 797 VA Computrace potentiostat/galvanostat from Metrohm (Herisau, Switzerland). The experiments were carried out with a typical three electrode cell: a glassy carbon rotating disk electrode (RDE) was used as working electrode (stirring rate 2000 rpm), a platinum rod electrode was employed as the counter electrode, and a Ag/AgCl electrode filled with 3 mol L^{-1} KCl was used as reference electrode. Solutions of the complexes for cyclic voltammetry measurements were prepared by dissolving solid samples of the complexes in 0.1 M KCl and purged with high purity (99.999%) nitrogen during 30 s prior recording the voltammograms. The starting and end potentials were −0.1 V, while the first vertex potential was set to −0.9 or −1.2 V depending on the potentials of the cathodic peaks.

Preparation of the complexes

General procedure. A solution of $Eu(NO_3)_3\cdot 5H_2O$ (0.0428 g, 0.1 mmol), $Gd(NO_3)\cdot 6H_2O$ (0.0451 g, 0.1 mmol) or $Tb(NO_3)_3\cdot 5H_2O$ (0.0435 g, 0.1 mmol) in methanol (5 mL) was added to a stirred solution of L^1(0.069 g, 0.1 mmol) in the same solvent (10 mL). The addition of the metal salt does not led to the precipitation of the complexes. Slow concentration of the methanolic solutions resulted in the formation of an oil which was dissolved in water. Slow evaporation of the aqueous solutions gave rise to precipitates which were isolated by filtration and dried.

$[EuL^1](NO_3)_3 \cdot 4H_2O$. Yield: 0.088 g (80%). IR (KBr, cm^{-1}): 1603 (m), 1459 (m), 1437 (m) [ν(C═C) and $\nu(C{=}N)_{py}$], 1324 (s), 828 (m), 761 (m) [$\nu(NO_3^-)$] [ν(NH)]. MS (ESI-MS, *m*/*z*, found (calculated)): 842 (841) $[Eu(L)-2H]^+$. $C_{42}H_{54}EuN_{13}O_{13}$ (1100.9): calcd C 45.8, H 4.9, N 16.5; found C 46.3, H 4.8, N 16.9. ^{1}H NMR (d_3-MeOD, 400 MHz, 25 °C, TMS): 25.38 (b, 4H), 20.77 (d, 4H, ^3J = 7.0 Hz), 18.03 (t, 4H, ^3J = 7.5 Hz), 14.47 (d, 4H, ^3J = 7.2 Hz), 3.47 (s, 4H), −2.15 (t, 2H, ^3J = 8.3 Hz), −2.94 (s, 4H), −7.92 (d, 4H, ^3J = 7.8 Hz), −9.31 (s, 4H), −26.30 (d, 4H, ^2J = 15.6 Hz), −26.85 (d, 4H, ^2J = 18.1 Hz), −32.93 (s, 4H).

$[GdL^1](NO_3)_3 \cdot 6H_2O$. Yield: 0.025 g (22%). IR (KBr, cm^{-1}): 1603 (m), 1459 (m), 1437 (m) [ν(C═C) and $\nu(C{=}N)_{py}$], 1324 (s), 828 (m), 762 (m) [$\nu(NO_3^-)$]. MS (ESI-MS, *m*/*z*, found (calculated)): 846 (846) $[Gd(L^1)-2H]^+$. $C_{42}H_{58}GdN_{13}O_{15}$ (1142.3): calcd C 44.2, H 5.1, N 15.9; found C 44.1, H 4.8, N 15.8.

$[TbL^1](NO_3)_3 \cdot 4H_2O$. Yield: 0.083 g (75%). IR (KBr, cm^{-1}): 1603 (m), 1459 (m), 1437 (m) [ν(C═C) and $\nu(C{=}N)_{py}$], 1324 (s), 828 (m), 761 (m) [$\nu(NO_3^-)$]. MS (ESI-MS, *m*/*z*, found (calculated)): 848 (847) $[Tb(L)-2H]^+$. $C_{42}H_{54}TbN_{13}O_{13}$ (1107.9): calcd C 45.5, H 4.9, N 16.4; found C 45.3, H 4.9, N 16.5.

Photophysical studies

UV-visible absorption spectra were recorded on a Specord 205 (Analytik Jena) spectrometer. Steady state emission and excitation spectra were recorded on a FLP920 spectrometer from Edinburgh Instruments working with a continuous 450 W Xe lamp and a red sensitive Hamamatsu R928 photomultiplier in Peltier housing. The emission spectrum of $[EuL^1]^{3+}$ was measured by using a nitrogen cooled Hamamatsu R5509-72 Vis-NIR (300–1700 nm) photomultiplier affording similar results. All spectra were corrected for the instrumental functions. When necessary, a 455 nm highpass filter was used to eliminate the second order artefacts.

Phosphorescence lifetimes were measured on the same instrument working in the Multi Channels Spectroscopy (MCS) mode and using a Xenon flash lamp as the excitation source. Errors on the luminescence lifetimes are estimated to ±10%. Hydrations numbers, *q*, were obtained using equation of Beeby *et al.*[17] Luminescence quantum yields were measured according to conventional procedures, with diluted solutions (optical density < 0.05), using $[Ru(bipy)_3]Cl_2$ in non-degassed water (Φ = 4.0%),[20] or Rhodamine 6G in water (Φ = 76.0%)[18] as references. Estimated errors are ±15%.

Computational studies

Full geometry optimisations of the $[EuL^1]^{3+}$ and $[EuL^2]^{3+}$ complexes were performed using DFT calculations with the TPSSh functional[41] and the Gaussian09 package.[42] The basis set employed for structure optimizations consisted of the large-core quasi-relativistic effective core potential (LCRECP) of Dolg *et al.* for Eu, which includes 46 + $4f^6$ electrons of Eu^{III} in the core, together with the associated (7s6p5d)/[5s4p3d]-GTO valence basis set,[43] and the standard 6-31G(d,p) basis set for all other atoms. The stationary points were characterised by frequency analysis. Since these calculations included the 4f electrons in the core, they were conducted in a pseudo-singlet configuration. Additional calculations were also performed using the LCRECP definition that includes 46 + $4f^7$ electrons in the core, using a doublet configuration. The lowest-energy ligand-centred triplet states were also obtained by geometry optimization using a pseudo-triplet configuration. Time-dependent density functional theory (TDDFT)[44] was used to calculate the 30 lowest energy singlet–singlet electronic transitions. Bulk solvent effects (water) were considered with the polarizable continuum model (PCM). Among the different implementations of the PCM we selected the integral equation formalism (IEFPCM),[45] together with universal force field radii (UFF)[46] scaled by a factor of 1.1, to define the solute cavities.

All-electron relativistic calculations were performed using the ORCA program package (Release 4.0.1.2)[47] with the second order Douglas–Kroll–Hess (DKH2) method.[48] The SARC2-DKH-QZVP[49] basis set was used for Eu, while the DKH-def2-TZVP basis set was used for C, H, N and O. The latter basis set

contains the exponents from the def2-TZVP basis set of Ahlrichs[50] and was re-contracted for DKH2 calculations by Pantazis *et al.*[51] The RIJCOSX approximation[52] was used to speed up calculations using the SARC2-DKH-QZVP/JK[49] auxiliary basis set for Eu and auxiliary basis sets for the remaining atoms generated automatically by ORCA using AutoAux procedure.[53] Solvent effects were introduced with the universal solvation model based on solute electron density and on a continuum model (SMD).[54]

Conflicts of interest

There are no conflicts to declare.

Acknowledgements

Authors C. P.-I. and D. E.-G. thank Ministerio de Economía y Competitividad (CTQ2016-76756-P) and Xunta de Galicia (ED431B 2017/59 and ED431D 2017/01) for generous financial support and *Centro de Supercomputación de Galicia* (CESGA) for providing the computer facilities. Authors A. M. N. and L. J. C. thank the French Centre National de la Recherche Scientifique and the University of Strasbourg for financial support.

References

01 (*a*) T. Nishioka, K. Fukui and K. Matsumoto, *Handbook on the Physics and Chemistry of Rare Earths*, K. A. Gschneider Jr., J.-C. G. Bünzli and V. K. Pecharsky, 2007, vol. 37, 171; (*b*) S. V. Eliseeva and J.-C. G. Bünzli, *Chem. Soc. Rev.*, 2010, **39**, 189; (*c*) J.-C. G. Bünzli *Chem. Rev.*, 2010, **110**, 2729; (*d*) N. Hildebrandt, L. J. Charbonnière and H.-G. Löhmannsröben, *J. Biomed. Biotechnol.*, 2007, 79169.

02 (*a*) M. Delbianco, V. Sadovnikova, E. Bourrier, G. Mathis, L. Lamarque, M. J. Zwier and D. Parker, *Angew. Chem., Int. Ed.*, 2014, **53**, 10718; (*b*) M. Starck, R. Pal and D. Parker, *Chem. – Eur. J.*, 2016, **22**, 570; (*c*) A. Picot, A. D'Aleo, P. L. Baldeck, A. Grichine, A. Duperray, C. Andraud and O. Maury, *J. Am. Chem. Soc.*, 2008, **130**, 1532; (*d*) C. P. Montgomery, B. S. Murray, E. J. New, R. Pal and D. Parker, *Acc. Chem. Res.*, 2009, **42**, 925; (*e*) A. T. Frawley, H. V. Linford, M. Starck, R. Pal and D. Parker, *Chem. Sci.*, 2018, **9**, 1042.

03 (*a*) U. Cho, D. Riordan, P. Ciepla, K. S. Kocherlakota, J. K. Chen and P. B. Harbury, *Nat. Chem. Biol.*, 2018, **14**, 15; (*b*) I. Martinic, S. V. Eliseeva, T. N. Nguyen, V. L. Pecoraro and S. Petoud, *J. Am. Chem. Soc.*, 2017, **139**, 8388; (*c*) M. Sy, A. Nonat, N. Hildebrandt and L. J. Charbonnière, *Chem. Commun.*, 2016, **52**, 5080.

04 T. Gunnlaugsson and J. P. Leonard, *Chem. Commun.*, 2005, 3114.

05 R. M. Supkowski and W. DeW. Horrocks Jr., *Inorg. Chim. Acta*, 2002, **340**, 44.

06 A. D'Aléo, F. Pointillart, L. Ouahab, C. Andraud and O. Maury, *Coord. Chem. Rev.*, 2012, **256**, 1604.

07 (*a*) S. Petoud, S. M. Cohen, J.-C. G. Bünzli and K. N. Raymond, *J. Am. Chem. Soc.*, 2003, **125**, 13324; (*b*) G.-L. Law, T. A. Pham, J. Xu and K. N. Raymond, *Angew. Chem., Int. Ed.*, 2012, **51**, 2371; (*c*) J.-C. G. Bünzli *Coord. Chem. Rev.*, 2015, **293–294**, 19; (*d*) A. T. Bui, A. Roux, A. Grichine, A. Duperray, C. Andraud and O. Maury, *Chem. – Eur. J.*, 2018, **24**, 3408; (*e*) M. Soulié, F. Latzko, E. Bourrier, V.

Placide, S. J. Butler, R. Pal, J. W. Walton, P. L. Baldeck, B. Le Guennic, C. Andraud, J. M. Zwier, L. Lamarque, D. Parker and O. Maury, *Chem. – Eur. J.*, 2014, **20**, 8636.

08 (*a*) C. Dee, D. Esteban-Gómez, C. Platas-Iglesias and M. Seitz, *Inorg. Chem.*, 2018, **57**, 7390; (*b*) E. S. Andreiadis, R. Demadrille, D. Imbert, J. Pecaut and M. Mazzanti, *Chem. – Eur. J.*, 2009, **15**, 9458; (*c*) R. Pal and D. Parker, *Chem. Commun.*, 2007, 474; (*d*) A. Dadabhoy, S. Faulkner and P. G. Sammes, *J. Chem. Soc., Perkin Trans. 2*, 2002, 348; (*e*) J. D. Routledge, M. W. Jones, S. Faulkner and M. Tropiano, *Inorg. Chem.*, 2015, **54**, 3337; (*f*) C. Yang, L.-M. Fu, Y. Wang, J.-P. Zhang, W.-T. Wong, X.-C. Ai, Y.-F. Qiao, B.-S. Zou and L.-L. Gui, *Angew. Chem., Int. Ed.*, 2004, **43**, 5010.

09 (*a*) D. Parker, R. S. Dickins, H. Puschmann, C. Crossland and J. A. K. Howard, *Chem. Rev.*, 2002, **102**, 1977; (*b*) G. J. Stasiuk and N. J. Long, *Chem. Commun.*, 2013, **49**, 2732.

10 P. Caravan, J. J. Ellison, T. J. McMurry and R. B. Lauffer, *Chem. Rev.*, 1999, **99**, 2293.

11 (*a*) N. Cakic, S. Gündüz, R. Rengarasu and G. Angelovski, *Tetrahedron Lett.*, 2015, **56**, 759; (*b*) F. Denat, S. Brandès and R. Guilard, *Synlett*, 2000, 561; (*c*) F. Oukhatar, M. Beyler and R. Tripier, *Tetrahedron*, 2015, **71**, 3857.

12 (*a*) A. Nonat, C. Gateau, P. H. Fries and M. Mazzanti, *Chem. – Eur. J.*, 2006, **12**, 7133; (*b*) A. Nonat, M. Giraud, C. Gateau, P. H. Fries, L. Helm and M. Mazzanti, *Dalton Trans.*, 2009, 8033; (*c*) A. T. Bui, A. Grichine, A. Duperray, P. Lidon, F. Riobé, C. Andraud and O. Maury, *J. Am. Chem. Soc.*, 2017, **139**, 7693; (*d*) A. T. Frawley, R. Pal and D. Parker, *Chem. Commun.*, 2016, **52**, 13349; (*e*) G. Tallec, P. H. Fries, D. Imbert and M. Mazzanti, *Inorg. Chem.*, 2011, **50**, 7943; (*f*) J. Salaam, L. Tabti, S. Bahamyirou, A. Lecointre, O. Hernandez Alba, O. Jeannin, F. Camerel, S. Cianférani, E. Bentouhami, A. Nonat and L. J. Charbonnière, *Inorg. Chem.*, 2018, **57**, 6095.

13 (*a*) H. Bazin, M. Preaudat, E. Trinquet and G. Mathis, *Spectrochim. Acta, Part A*, 2001, **57**, 2197; (*b*) J. M. Zwier, H. Bazin, L. Lamarque and G. Mathis, *Inorg. Chem.*, 2014, **53**, 1854; (*c*) S. Faulkner, A. Beeby, M.-C. Carrie, A. Dadabhoy, A. M. Kenwright and P. G. Sammes, *Inorg. Chem. Commun.*, 2001, **4**, 187; (*d*) F. Bodar-Houillon, R. Heck, W. Bohnenkamp and A. Marsura, *J. Lumin.*, 2002, **99**, 335; (*e*) V. Korovin, N. V. Rusakova and A. Popkov, *J. Appl. Spectrosc.*, 2002, **69**, 89; (*f*) C. Doffek, N. Alzakhem, M. Molon and M. Seitz, *Inorg. Chem.*, 2012, **51**, 4539; (*g*) C. Doffek, J. Wahsner, E. Kreidt and M. Seitz, *Inorg. Chem.*, 2014, **53**, 3263; (*h*) C. Doffek, N. Alzakhem, C. Bischof, J. Wahsner, T. Güden-Silber, J. Lügger, C. Platas-Iglesias and M. Seitz, *J. Am. Chem. Soc.*, 2012, **134**, 16413.

14 M. del C. Fernández-Fernández, R. Bastida, A. Macías, P. Pérez-Lourido, C. Platas-Iglesias and L. Valencia, *Inorg. Chem.*, 2006, **45**, 4484–4496.

15 G. Castro, M. Regueiro-Figueroa, D. Esteban-Gómez, R. Bastida, A. Macías, P. Pérez-Lourido, C. Platas-Iglesias and L. Valencia, *Chem. – Eur. J.*, 2015, **21**, 18662.

16 G. Castro, M. Regueiro-Figueroa, D. Esteban-Gómez, P. Pérez-Lourido, C. Platas-Iglesias and L. Valencia, *Inorg. Chem.*, 2016, **55**, 3490.

17 A. Beeby, I. M. Clarkson, R. S. Dickins, S. Faulkner, D. Parker, L. Royle, A. S. de Sousa, J. A. G. Williams and M. Woods, *J. Chem. Soc., Perkin Trans. 2*, 1999, 493.

18 J. Olmsted *J. Phys. Chem.*, 1979, **83**, 2581.

19 R. Tripier, C. Platas-Iglesias, A. Boos, J.-F. Morfin and L. J. Charbonnière, *Eur. J. Inorg. Chem.*, 2010, 2735.

20 H. Ishida, S. Tobita, Y. Hasegawa, R. Katoh and K. Nozaki, *Coord. Chem. Rev.*, 2010, **254**, 2449.

21 (*a*) K. Binnemans *Coord. Chem. Rev.*, 2015, **295**, 1; (*b*) M. H. V. Wertz, R. T. J. Jukes and J. W. Verhoeven, *Phys. Chem. Chem. Phys.*, 2002, **4**, 1542.

22 (*a*) C. C. Bryden and C. N. Reilley, *Anal. Chem.*, 1982, **54**, 610; (*b*) M. Albin, W. DeW. Horrocks Jr. and F. J. Liotta, *Chem. Phys. Lett.*, 1982, **85**, 61.

23 P. A. Tanner *Chem. Soc. Rev.*, 2013, **42**, 5090.

24 R. A. Sa Ferreira, S. S. Nobre, C. M. Granadeiro, H. I. S. Nogueira, L. D. Carlos and O. L. Malta, *J. Lumin.*, 2006, **121**, 561.

25 A. Nonat, M. Regueiro-Figueroa, D. Esteban-Gomez, A. de Blas, T. Rodriguez-Blas, C. Platas-Iglesias and L. J. Charbonnière, *Chem. – Eur. J.*, 2012, **18**, 8163.

26 L. Valencia, J. Martinez, A. Macías, R. Bastida, R. A. Carvalho and C. F. G. C. Geraldes, *Inorg. Chem.*, 2002, **41**, 5300.

27 M. T. Berry, P. S. May and H. Xu, *J. Phys. Chem.*, 1996, **100**, 9216.

28 S. Petoud, J.-C. G. Bünzli, T. Glanzman, C. Piguet, Q. Xiang and R. P. Thummel, *J. Lumin.*, 1999, **82**, 69.

29 L. J. Charbonnière, C. Balsiger, K. J. Schenk and J.-C. G. Bünzli, *Dalton Trans.*, 1998, 505.

30 N.-D. H. Gamage, Y. Mei, J. Garcia and M. J. Allen, *Angew. Chem., Int. Ed.*, 2010, **49**, 8923.

31 M. Regueiro-Figueroa, J. L. Barriada, A. Pallier, D. Esteban-Gómez, A. de Blas, T. Rodríguez-Blas, E. Tóth and C. Platas-Iglesias, *Inorg. Chem.*, 2015, **54**, 4940.

32 L. Burai, É. Tóth, G. Moreau, A. Sour, R. Scopelliti and A. E. Merbach, *Chem. – Eur. J.*, 2003, **9**, 1394.

33 (*a*) M. Regueiro-Figueroa, D. Esteban-Gómez, A. de Blas, T. Rodríguez-Blas and C. Platas-Iglesias, *Chem. – Eur. J.*, 2014, **20**, 3974; (*b*) M. Regueiro-Figueroa and C. Platas-Iglesias, *J. Phys. Chem. A*, 2015, **119**, 6436.

34 D. Guillaumon, H. Bazin, J.-M. Benech, M. Boyer and G. Mathis, *ChemPhysChem*, 2007, **8**, 480.

35 M. Andrews, A. J. Amoroso, L. H. Harding and S. J. A. Pope, *Dalton Trans.*, 2010, **39**, 3407.

36 M. Dolg, H. Stoll and H. Preuss, *J. Chem. Phys.*, 1989, **90**, 1730.

37 (*a*) J.-H. Lan, W.-Q. Shi, L.-Y. Yuan, Y.-L. Zhao, J. Li and Z.-F. Chai, *Inorg. Chem.*, 2011, **50**, 9230; (*b*) B. Sadhu, M. Sundararajan and T. Bandyopadhyay, *Inorg. Chem.*, 2016, **55**, 598.

38 A. S. Ivanov and V. S. Bryantsev, *Eur. J. Inorg. Chem.*, 2016, 3474.

39 G. Blasse, M. Buys and N. Sabbatini, *Chem. Phys. Lett.*, 1986, **124**, 538.

40 D. Parker *Coord. Chem. Rev.*, 2000, **205**, 109.

41 J. M. Tao, J. P. Perdew, V. N. Staroverov and G. E. Scuseria, *Phys. Rev. Lett.*, 2003, **91**, 146401.

42 M. J. Frisch, *et al.*, Gaussian, Inc., Wallingford CT, 2009.

43 M. Dolg, H. Stoll, A. Savin and H. Preuss, *Theor. Chim. Acta*, 1989, **75**, 173–194.

44 (*a*) R. E. Stratmann, G. E. Scuseria and M. J. Frisch, *J. Chem. Phys.*, 1998, **109**, 8218; (*b*) R. Bauernschmitt and R. Ahlrichs, *Chem. Phys. Lett.*, 1996, **256**, 454; (*c*) M. E. Casida, C. Jamorski, K. C. Casida and D. R. Salahub, *J. Chem. Phys.*, 1998, **108**, 4439.

45 J. Tomasi, B. Mennucci and R. Cammi, *Chem. Rev.*, 2005, **105**, 2999.

46 A. K. Rappe, C. J. Casewit, K. S. Colwell and W. A. Goddard, *J. Am. Chem. Soc.*, 1992, **114**, 10024.

47 F. Neese *Wiley Interdiscip. Rev.: Comput. Mol. Sci.*, 2012, **2**, 73.

48 (*a*) M. Barysz and A. J. Sadlej, *J. Mol. Struct.*, 2001, **573**, 181; (*b*) M. Reiher *Theor. Chem. Acc.*, 2006, **116**, 241.

49 D. Aravena, F. Neese and D. A. Panzatis, *J. Chem. Theory Comput.*, 2016, **12**, 1148.

50 F. Weigend and R. Ahlrichs, *Phys. Chem. Chem. Phys.*, 2005, **7**, 3297.

51 D. A. Pantazis, X.-Y. Chen, C. R. Landis and F. Neese, *J. Chem. Theory Comput.*, 2008, **4**, 908.

52 (*a*) F. Neese, F. Wennmohs, A. Hansen and U. Becker, *Chem. Phys.*, 2009, **356**, 98; (*b*) R. Izsak and F. Neese, *J. Chem. Phys.*, 2011, **135**, 144105; (*c*) T. Petrenko, S. Kossmann and F. Neese, *J. Chem. Phys.*, 2011, **134**, 054116; (*d*) S. Kossmann and F. Neese, *Chem. Phys. Lett.*, 2009, **481**, 240.

53 G. L. Stoychev, A. A. Auer and F. Neese, *J. Chem. Theory Comput.*, 2017, **13**, 554.

54 A. V. Marenich, C. J. Cramer and D. G. Truhlar, *J. Phys. Chem. B*, 2009, **113**, 6378.

[i] Electronic supplementary information (ESI) available: ^{1}H NMR spectra, absorption and emission spectra, cyclic voltammograms and optimized Cartesian coordinates obtained with DFT calculations. See DOI: 10.1039/c8dt05005h.